



# Stereo-vision-based AUV navigation system for resetting the inertial navigation system error

Hong Yi Hsu<sup>1</sup> · Yuichiro Toda<sup>1</sup> · Kohei Yamashita<sup>1</sup> · Keigo Watanabe<sup>1</sup> · Masahiko Sasano<sup>2</sup> · Akihiro Okamoto<sup>2</sup> · Shogo Inaba<sup>2</sup> · Mamoru Minami<sup>1</sup>

Received: 6 August 2021 / Accepted: 19 November 2021  
© International Society of Artificial Life and Robotics (ISAROB) 2021

## Abstract

The Autonomous Underwater Vehicle (AUV) is used for underwater exploration of the sea floor. The AUV uses an Inertial Navigation System (INS) to recognize its position in the water, through the position estimation error of the INS increases with time. As the INS accumulated error increases, the success rate of the task decreases. Global Positioning System (GPS) is used for all kinds of vehicles moving on the ground or in the air; however, it cannot be widely utilized in water because radio signals cannot penetrate into the deep water. Therefore, how to eliminate the INS error is an important topic for the AUV. In this study, we propose a stereo-vision-based navigation system applied to the AUV to reset the integrated INS error. The experiments of the AUV navigation and returning to the docking station were conducted in the test tank by means of the INS and the stereo-vision system. The experimental results show that our proposed method is capable of docking the AUV and resetting the integrated INS error.

**Keywords** Visual servoing · Real-time multi-step GA · AUV · Docking · Stereo-vision camera · INS

## 1 Introduction

Underwater vehicles are used for tracing submarine cables, surveying submarines, and inspecting the underwater structures [1–3]. All of these tasks require considerable working time underwater. In those underwater tasks, two main types of underwater vehicles are used: Remotely Operated Vehicle (ROV) and Autonomous Underwater Vehicle (AUV). Both of those underwater vehicles rely on different types of power sources. ROV uses cables to obtain power from the ground or from the mother ship, while AUV uses a battery to obtain power. In terms of the ROV, the cable could be damaged by friction with rocks on the sea floor, and the tension of the

several-thousand-meter cable adversely affects the navigation of the vehicle in deep sea. Although the AUV does not have the cable problem, its operation time is limited by the battery capacity. When AUV has a continuous electricity supply, it can perform underwater tasks better than ROV. To ensure the continuity of the electricity supply for AUV, in this study, an underwater docking function is used to recharge the battery.

There are three stages in the recharging operation: (1) long-distance navigation, (2) approach, and (3) short-distance docking. While returning to the docking station for recharging battery, AUV utilizes the navigation system, such as the Inertial Navigation System (INS) and sonar sensors. To recharge the battery successfully, the charging plug of the AUV and the charging socket of the docking station must be mechanically coupled. Therefore, the control system requires a high level of positioning precision in order to achieve the docking operation. However, the positioning precision of both INS and sonar sensors is not enough to achieve such docking operations [4–6]. Besides, the INS has the greatest defect that the error accumulates with time. To improve the positioning precision and correct the defect, the INS must work in tandem with another system, such as GPS or Doppler Velocity

---

This work was presented in part at the 26th International Symposium on Artificial Life and Robotics (Online, January 21–23, 2021).

---

✉ Hong Yi Hsu  
pcvv4h2h@s.okayama-u.ac.jp

<sup>1</sup> Present Address: Okayama University, 1-1-1 Tsushimanaka, Kita Ward 700-8530, Okayama, Japan

<sup>2</sup> National Maritime Research Institute, 6-38-1 Shinkawa, Mitaka 181-0004, Tokyo, Japan

Log (DVL). However, the GPS signals do not reach to the deep sea, and the DVL shows the distance and relative velocity to the seafloor, but not the absolute position. As for the AUV normal navigation system used in the underwater task, the success rate of the task decreases as the INS accumulated error increases. In order to perform the underwater recharging operation, two requirements must be fulfilled: (1) the elimination of integrated INS error also called dead-reckoning error, (2) the improvement of positioning accuracy of the control system.

There are many studies on the high precision of the underwater recharging system [7–10]. Our research team used a stereo-vision-based navigation system to realize high accuracy docking control system [11–16]. [11–14] verify the stability of the proposed stereo-vision-based navigation system in a simulation pool and have performed docking operation in the real sea environment. [15, 16] confirmed the feasibility area of the proposed system for the docking operation in the simulation pool with different turbidity and distance. To conclude, the previous studies provide an effective method to perform the docking operation. However, those previous works focus on only docking operation, but the point that the docking means is not only for recharging of battery but also resetting the integrated INS errors. Therefore, in this study, the proposed stereo-vision-based navigation system has been integrated in the AUV navigation system to confirm the practicality of the AUV system. The shortcoming of the AUV navigation system is related to the accumulated INS errors. The INS errors has been firstly and practically confirmed to be eliminated using real AUV by resetting the accumulated integration error of dead-reckoning navigation system, which enable the AUV to navigate itself by dead-reckoning in an extent with the integration errors being kept low than certain allowable errors. This is the point of this paper to be evaluated.

Since the underwater vehicle used in this study is different from previous ones, the stability of the proposed system used on the AUV must be verified by two preliminary experiments. One is an iterative docking experiment to confirm that the proposed system of the AUV is functioning properly. Ocean currents in the real sea environment disturb the AUV; thus, the other experiment tests the robustness of the AUV, especially when the AUV is affected by an external force during the docking operation. Next, the comprehensive experiment simulates the process of AUV performing a recharging operation. The AUV uses a normal navigation system to approach the docking station, and then it uses a stereo-vision-based navigation system to complete the docking operation. The experimental results show that the proposed system for the AUV allows its underwater movement and docking. Also, the integrated INS error is reset after the AUV completes the docking operation.

## 2 Hardware for the recharging operation

The hardware used in this study is divided into three parts: Recognition Unit, AUV, Docking Station with lighting 3D Marker. The experiment simulates a realistic recharging operation by inserting three docking poles on the AUV into three docking holes on the docking station. The hardware for the recharging operation is explained in this section.

### 2.1 Recognition unit

In our proposed recognition system, the real-time pose estimation method is composed of the 3D model-based matching method and the Real-time Multi-step Genetic Algorithm(RM-GA) [17], so that a target object will be recognized by stereo vision. The recognition program is installed on the computer called GA-PC, has shown in Fig. 1b. The GA-PC that processes camera signals and sends operational instructions to the AUV is installed in a pressure container. Two interface boards are used in the GA-PC to receive images from the stereo-vision camera on the AUV. Figure 1a shows the overall block diagram for the proposed system. By using the real-time estimated relative pose between the AUV and the target object, GA-PC sends maneuver command signals to the AUV via TCP/IP.

### 2.2 Autonomous underwater vehicle

This study uses the hovering-AUV named as Hobalin, which has been developed by the National Maritime Research Institute Japan in the project of SIP[18, 19]. As shown in Fig. 2,  $\Sigma_H$  is the coordinate system of the AUV, and the origin is the center point between the two cameras. The specification of the AUV is shown in Table 1. In the docking operation, the stereo-vision camera and three docking poles are attached

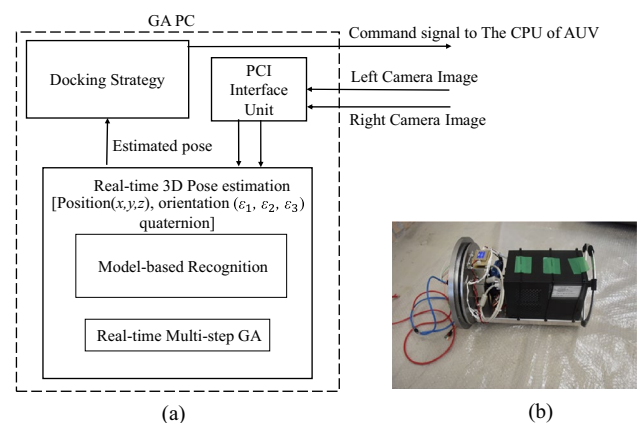


**Fig. 1** **a** Block diagram of the proposed system and **b** Photo of the GA-PC

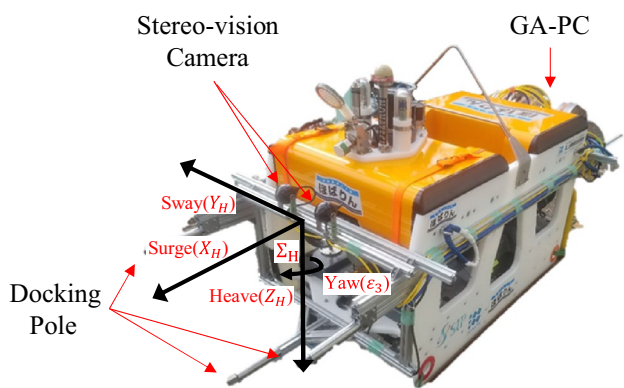


Fig. 2 The hovering Autonomous Underwater Vehicle Hobalin with the Stereo-vision-based navigation system

Table 1 Specifications of the AUV Hobalin

Max. depth [m]	2000
Dimensions [mm]	1200 × 700 × 760
Weight [kg]	270
Duration [h]	8
Number of thrusters	Horizontal thruster × 4 Vertical thruster × 2
Navigation sensor	INS, DVL, Sheet Laser Pressure gauge, GPS antenna(AIR) Surveillance camera(forward)
Observation sensors	Turbidimeter, CT Sensor, pH Sensor Profiling sonar, Observation cameras
Other equipments	Iridium beacon, LED flasher Acoustic positioning transponder, Ballast releasers

to the front of the AUV. The GA-PC installed in a pressure container is fixed to the rear of the AUV.

### 2.3 Docking station with lighting 3D Marker

The unidirectional docking station is designed to demonstrate underwater battery recharging, as shown in Fig. 3. The docking station is 0.60 m long × 0.45 meter wide × 3 m high in size. The docking station with a lighting 3D marker and three docking holes is fixed in the test tank. Each docking pole and each docking hole are mechanically coupled to each other.

The lighting 3D marker installed on the docking station is used as the target object for the docking operation, as shown in Fig. 4. The 3D marker has three spheres in red, green, and blue respectively. Each sphere with a built-in LED is 40 millimeters in diameter. The power supply for the LED is 12 volts DC. The 3D marker gets power directly from the docking station when the docking station is installed on the seabed. To

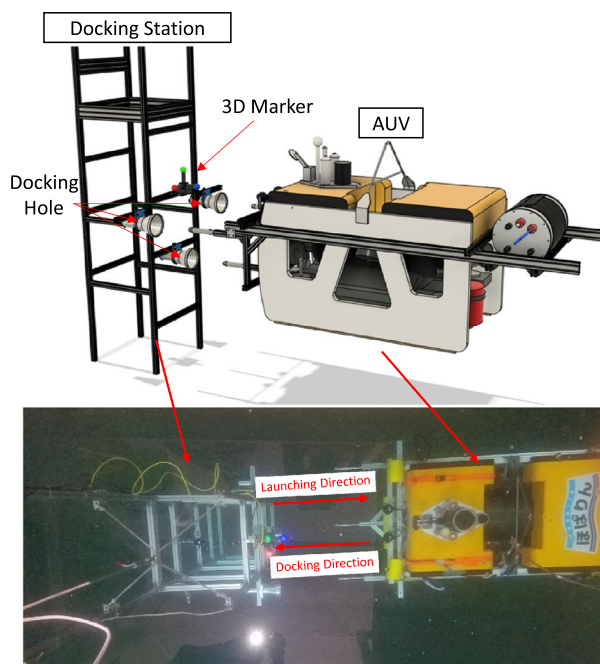


Fig. 3 The docking station for the docking operation

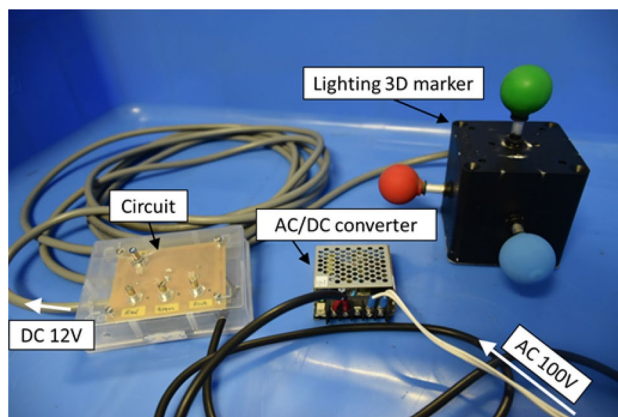


Fig. 4 The 3D marker has three spheres in red, green, and blue respectively

perform the docking experiment in different environment, a variable resistance is incorporated in the circuit to adjust the brightness of each color. This allows the 3D marker to be used at different illumination environments.

### 3 Software for the recharging operation

The real-time pose estimation method with RM-GA has been developed for the docking operation by our previous works [17]. In this section, the method is briefly discussed for the reader's convenience.

### 3.1 3D model-based matching method

Feature-based recognition uses 2D-to-3D reconstruction calculations, for the information about the target object is determined by a set of points in different images. If a point in one image is incorrectly mapped to another point in another image, the pose of the reconstructed object does not represent the real 3D object’s pose. A pose estimation method with 3D-to-2D model projection is used in this study because forward projection from 3D-to-2D generates a unique point in the 2D image without any errors [20].

With the 3D-to-2D approach, a model-based matching method is used to recognize the 3D marker and to estimate its pose in real time. The model-based matching method utilizes the known shape, color and size of the 3D marker. The poses of the assumed models are predefined and distributed in the 3D search space in front of the stereo-vision camera. Each assumed model is then projected onto the two camera images, as shown in Fig. 5, in which  $\Sigma_M$  is the 3D marker coordinate system for the proposed system.  $\Sigma_{M_i}$  is the  $i$ -th assumed model coordinate system.  $\Sigma_{CL}$  and  $\Sigma_{CR}$  are the left and right camera coordinate systems.  $\Sigma_{IL}$  and  $\Sigma_{IR}$  are the left and right image coordinate systems. The  $j$ -th point on the  $i$ -th assumed model in the 3D search space is projected onto the left and right camera images, and these poses are calculated by using the projection geometry. Finally, the best assumed model (mostly overlapping the 3D marker) that represents the true pose has the highest fitness value.

### 3.2 Real-time multi-step genetic algorithm

The problem of recognizing the 3D marker and detecting its pose is converted into an optimization problem of a multi-peak distribution, which is the calculation result of the fitness function. The calculation result of the fitness function, i.e., fitness value, is used to evaluate the correlation between the

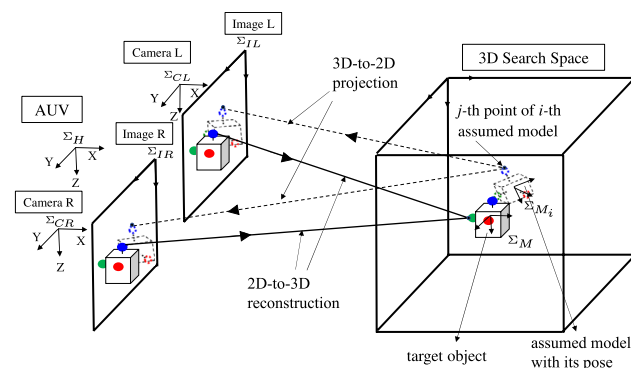


Fig. 5 3D model-based matching system with a stereo-vision camera, using 3D-to-2D projection and 2D-to-3D reconstruction

3D marker and the  $i$ -th assumed model with its pose  $\phi_i$  in the captured image [21, 22].  $\phi_i$  means the pose of the  $i$ -th assumed model given by the RM-GA. Figure 6 shows the 3D marker projected onto the image plane and the dotted circle, i.e., the  $i$ -th assumed model, obtained from the 3D-to-2D projection onto the same image plane. Each assumed model consists of the red, green, and blue balls. Each ball of the assumed model comprises an inner sphere  $S_{in}$  and an enveloping sphere  $S_{out}$ . The inner sphere  $S_{in}$  is intended to evaluate the ball area of the 3D marker, and the enveloping sphere  $S_{out}$  is for the background area. The fitness function used in the proposed method is defined as the following:

$$F(\phi_i) = \frac{1}{2}(F_L(\phi_i) + F_R(\phi_i))$$

$$F_L(\phi_i) = \frac{1}{N} \left( \sum_{{}^{IL}r_j(\phi_i) \in S_{L,in}(\phi_i)} p({}^{IL}r_j(\phi_i)) - \sum_{{}^{IL}r_j(\phi_i) \in S_{L,out}(\phi_i)} p({}^{IL}r_j(\phi_i)) \right)$$

$$F_R(\phi_i) = \frac{1}{N} \left( \sum_{{}^{IR}r_j(\phi_i) \in S_{R,in}(\phi_i)} p({}^{IR}r_j(\phi_i)) - \sum_{{}^{IR}r_j(\phi_i) \in S_{R,out}(\phi_i)} p({}^{IR}r_j(\phi_i)) \right) \tag{1}$$

The fitness function for the  $i$ -th assumed model  $F(\phi_i)$  is calculated by averaging the fitness functions of both the left camera image  $F_L(\phi_i)$  and right camera image  $F_R(\phi_i)$ . The summation in Eq. (1) is related to the  $j$ -th point  ${}^{IL}r_j(\phi_i)$  in the left camera image, defined on the  $i$ -th assumed model

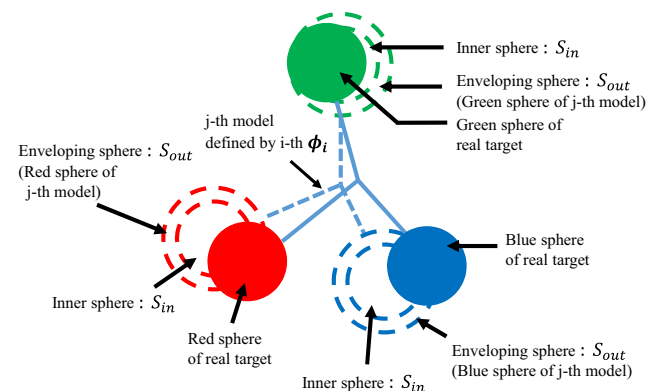


Fig. 6 Left or right camera’s 2D image of the real 3D marker and model

with pose  $\phi_i$ . The score of each point is evaluated by means of Eq. (1), where  $N$  represents the number of points to be evaluated. In this study,  $N$  is set at 50.

As shown in Fig. 7, there is a total of 60 points (36 points in the inner sphere  $S_{in}$  and 24 points in the enveloping sphere  $S_{out}$ ). In the projection, the diameter of the inner sphere is the same as that of the real sphere. When the two conditions are fulfilled, the fitness function increase that has a value of  $p({}^{ll}r_j(\phi_i)) = +1$  in Eq. (1). The conditions are (1) the  $j$ -th point  ${}^{ll}r_j(\phi_i)$  of  $i$ -th assumed model  $\phi_i$  in the inner sphere  $S_{in}$  overlaps the 3D marker and (2) the assumed model's hue color value coincides with the projected 3D marker's hue value. In this study, the hue ranges of left and right cameras are set as Table 2.

On the other hand, if the two conditions above do not satisfy together, the fitness function has a value of  $p({}^{ll}r_j(\phi_i)) = -1$ . This situation makes the fitness value decreases. Therefore, when the assumed model and the 3D marker completely overlap, the fitness value reaches the maximum, i.e., 1. The highest peak in the fitness distribution represents the true pose of the 3D marker. In [15, 16], when fitness value is over 0.3, it means that the proposed system can correctly recognize the 3D marker. Thus, the RM-GA solves the optimization problem in real time.

The RM-GA, is used to estimate the relative pose between the AUV and the 3D marker. The right part of Fig. 8 shows the flowchart of the RM-GA. A random population of assumed models in different poses is generated in the 3D search space. The stereo-vision camera captures a new pair of images on both left and right sides every 33 [ms]. The GA procedure is performed repetitively every 33 [ms] in every image. The latest evolution is then forwarded to the next step as the initial assumed model of the next new evolution, which is closer to the 3D marker projected naturally to the camera images. The RM-GA performs this procedure repeatedly to search for the

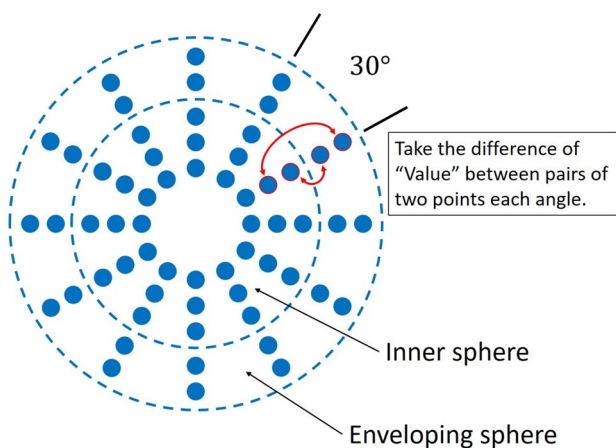


Fig. 7 Projection of the blue sphere of a model with selected sample points

Table 2 Hue ranges of left and right cameras that are detected and calculated as red, green and blue in fitness function

		Red	Green	Blue
Right camera	$h_{min}$	160	260	0
	$h_{max}$	200	320	60
Left camera	$h_{min}$	160	250	20
	$h_{max}$	200	340	70

best solution that represents the correct pose of the 3D marker. The convergence behavior of the GA procedure, from the first evolution to the final one, is shown in the left part of Fig. 8.

### 3.3 Docking control

The AUV is operated with a proportional controller. The six thrusters mounted on the AUV are controlled by sending a command voltage based on the feedback of the relative pose between the AUV and the 3D marker. The velocity of each axis is determined by the following equations:

$$Yaw : V_1 = k_{p1}(\epsilon_{3d} - \hat{\epsilon}_3) \tag{2}$$

$$Surge : V_2 = k_{p2}(x_d - \hat{x}) \tag{3}$$

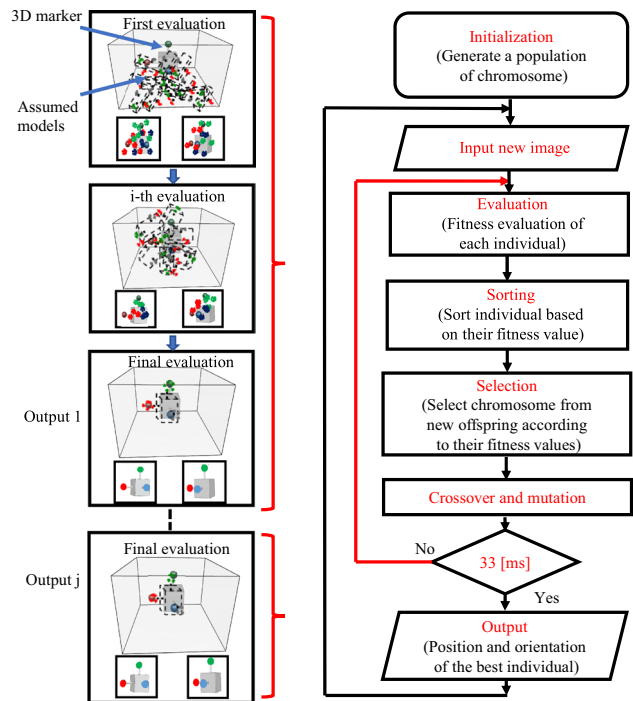


Fig. 8 Flowchart for the RM-GA: the terminal condition is defined as 33 [ms] because the video frame rate is 30 frames per second for the proposed system

$$\text{Sway} : V_3 = k_{p3}(y_d - \hat{y}) \quad (4)$$

$$\text{Heave} : V_4 = k_{p4}(z_d - \hat{z}) \quad (5)$$

$(\varepsilon_{3d}, x_d, y_d, z_d)$  is the relative desired pose between the AUV and the 3D marker.  $(\hat{\varepsilon}_3, \hat{x}, \hat{y}, \hat{z})$  is the relative estimated pose between the AUV the 3D marker.  $(k_{p1}, k_{p2}, k_{p3}, k_{p4})$  is defined as the gain for each deviation. In this paper, the value of the gain is set to  $(k_{p1}, k_{p2}, k_{p3}, k_{p4}) = (0.4, 0.5, 0.4, 1.0)$ .

### 3.4 Docking conditions

As for the proposed system in this study, if the docking conditions are fulfilled, the desired value in the surge direction decreases. The range of docking conditions on the sway and the heave depends on the distance between the AUV and the 3D marker. The docking condition range  $r_i$  of the  $i$ -axis is calculated as the following equation:

$$r_i = \frac{r_s - r_f}{d_s - d_f} x - \frac{r_s d_f - r_f d_s}{d_s - d_f} \quad (6)$$

where  $r_s$  and  $r_f$  represent the range of the docking conditions at the start and end points of the docking operation.  $d_s$  and  $d_f$  represent the start and end distances of docking operation. The range of docking conditions is determined by the distance  $x$  between the AUV and the 3D marker. If the conditions  $|y_d - \hat{y}| < r_y$  [mm],  $|z_d - \hat{z}| < r_z$  [mm], and  $|\varepsilon_{3d} - \hat{\varepsilon}_3| < 5$  [°] are satisfied, the desired value of the surge direction  $x_d = d_s - 30t$  [mm] decreases with time  $t$ , and the range of the docking conditions changes as the AUV moves forward.

## 4 Experiments using the AUV

Three experiments were conducted: an iterative docking operation, a docking operation under the influence of an external force, and a recharging operation by means of the AUV normal navigation system and the stereo-vision-based navigation system. The experiments were conducted in the test tank of the National Maritime Research Institute. The experimental environment is shown in Fig. 9.

### 4.1 First preliminary experiment: iterative docking experiment

The first preliminary experiment is an iterative docking experiment to confirm that the proposed system of the AUV with the stereo-vision can complete the docking operation. The AUV was manually guided to the front of the docking station until the 3D marker was in the field of view (at a distance of approximately 950 [mm] from the 3D marker in

the surge direction). Visual servoing then proceeded until the AUV achieved a stable pose for 165 [ms] within the docking conditions. When the AUV fulfilled the docking conditions, it began to insert the docking poles into the docking holes. It gradually decreased the surge distance between the AUV and 3D marker until it reached  $d_f = 220$  [mm]. When the docking operation was completed, the AUV returned to the distance of  $d_s = 600$  [mm] from the 3D marker for the next docking iteration.

Figure 10 shows the result of the 10-times iterative docking experiment. The fitness value of the iterative docking experiment is shown in Fig. 10a. All the fitness values are over 0.3, showing the system can correctly recognize the 3D marker. Figure 10b–e show the estimated and desired poses of the AUV in each axis. Among these figures, the black line is the estimated position, the red dotted line is the desired position, and the red line is the error allowance range. The one-time docking operation means AUV reaches 220 [mm] in the surge direction. As shown in Fig. 10b, the continuous iterative docking has been successfully conducted 10 times. In Fig. 10c–e, the experimental results show that almost all the estimated positions are within the error allowance range. Even though in Fig. 10e, some estimated positions are out of the error allowance range (50 [s]:  $-6.4^\circ$ , 83 [s]:  $5.1^\circ$ , 112 [s]:  $5.8^\circ$ , 228 [s]:  $5.5^\circ$ , and 290 [s]:  $5.3^\circ$ ), the poses of the AUV are immediately corrected to make the docking operation continue to perform. This means that the AUV can complete the iterative docking experiment smoothly by using our proposed system.

The fourth operation is analyzed in detail to elaborate on the movement of the AUV, as shown in Fig. 11. The docking operation is divided into five periods to be analyzed, from Fig. 11a, e. The corresponding photographs

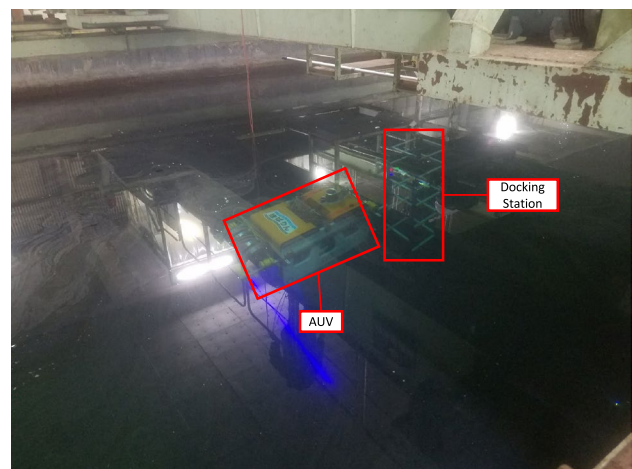
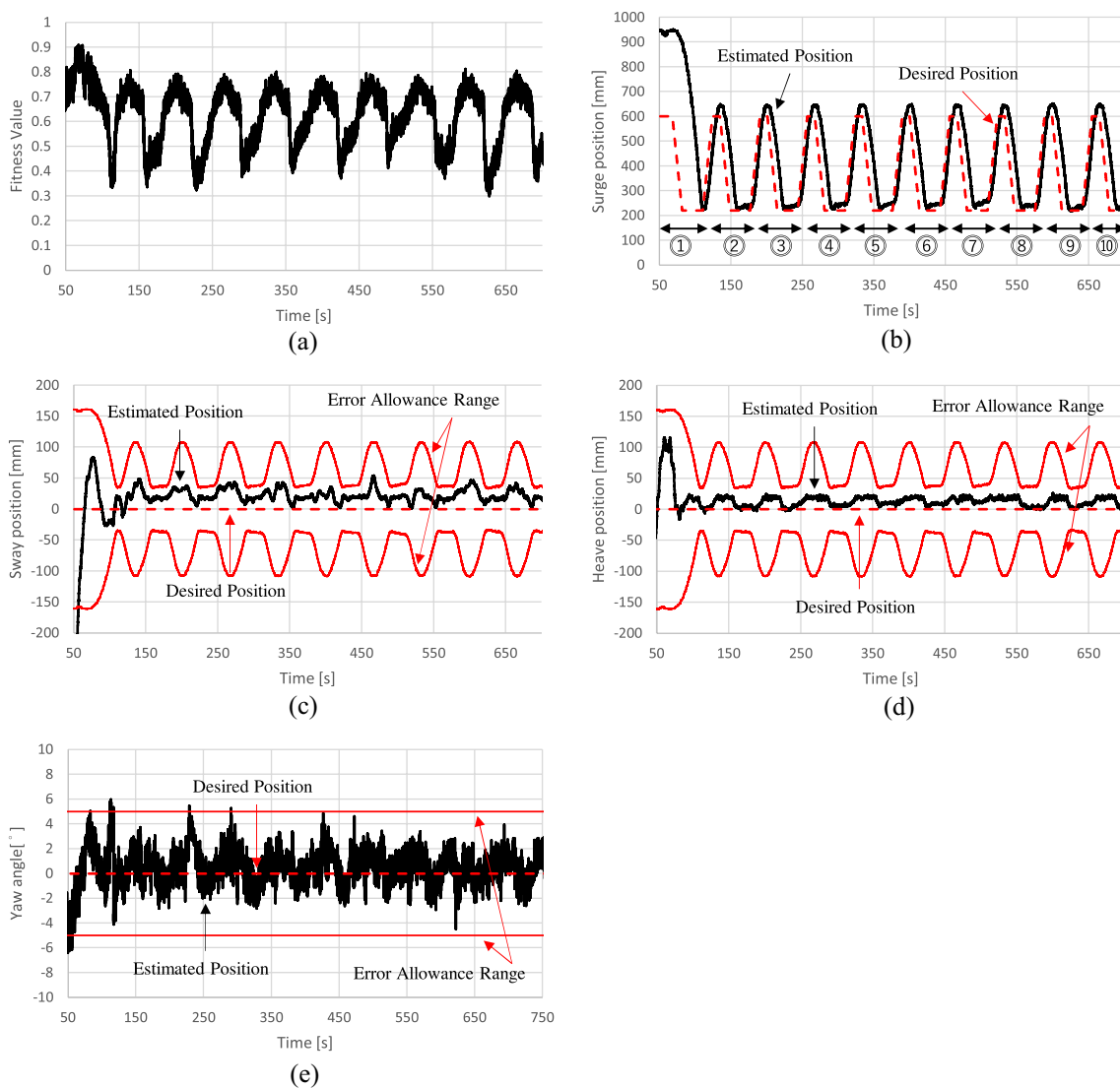


Fig. 9 The experimental environment for the AUV in the test tank with clear still water



**Fig. 10** 10-times Iterative docking experiment: (a) fitness value, (b) surge position, (c) sway position, (d) heave position and (e) yaw angle

during periods (a) - (e) are shown in the right part of Fig. 11. In Fig. 11a, the AUV has finished the 3rd docking operation and is about to return to the distance of 600 [mm] in the surge direction for the next docking iteration(Fig. 11b). At this moment, the estimation position in the surge direction is 393.3 [mm], and the desired position in the surge direction is 491 [mm]. The AUV is supposed to move forwards, but it moves backwards, as shown in Fig. 11c; the desired position in the surge direction is 516 [mm], while the estimation position in the surge direction is 642.6 [mm]. Since the proposed system is a proportional controller, there is an inertial force that creates an overshoot despite the fact that the AUV has reached the desired position. In Fig. 11d, after the AUV has overcome the effects of the inertial forces, the AUV starts to move forwards. In Fig. 11e, the AUV

reaches the target point. In this way, the docking operation experiment can be successfully performed by using our proposed stereo-vision system.

**4.2 Second preliminary experiment: docking operation under the influence of an external force**

The real sea environment is different from that in a test tank filled with still water because waves and ocean currents cause external forces which disturb the AUV. The second preliminary experiment verified that the AUV can completed the docking operation when subjected to external forces.

Figure 12 shows the experimental result of the AUV under the influence of an external force during the docking operation. The start and end points of the

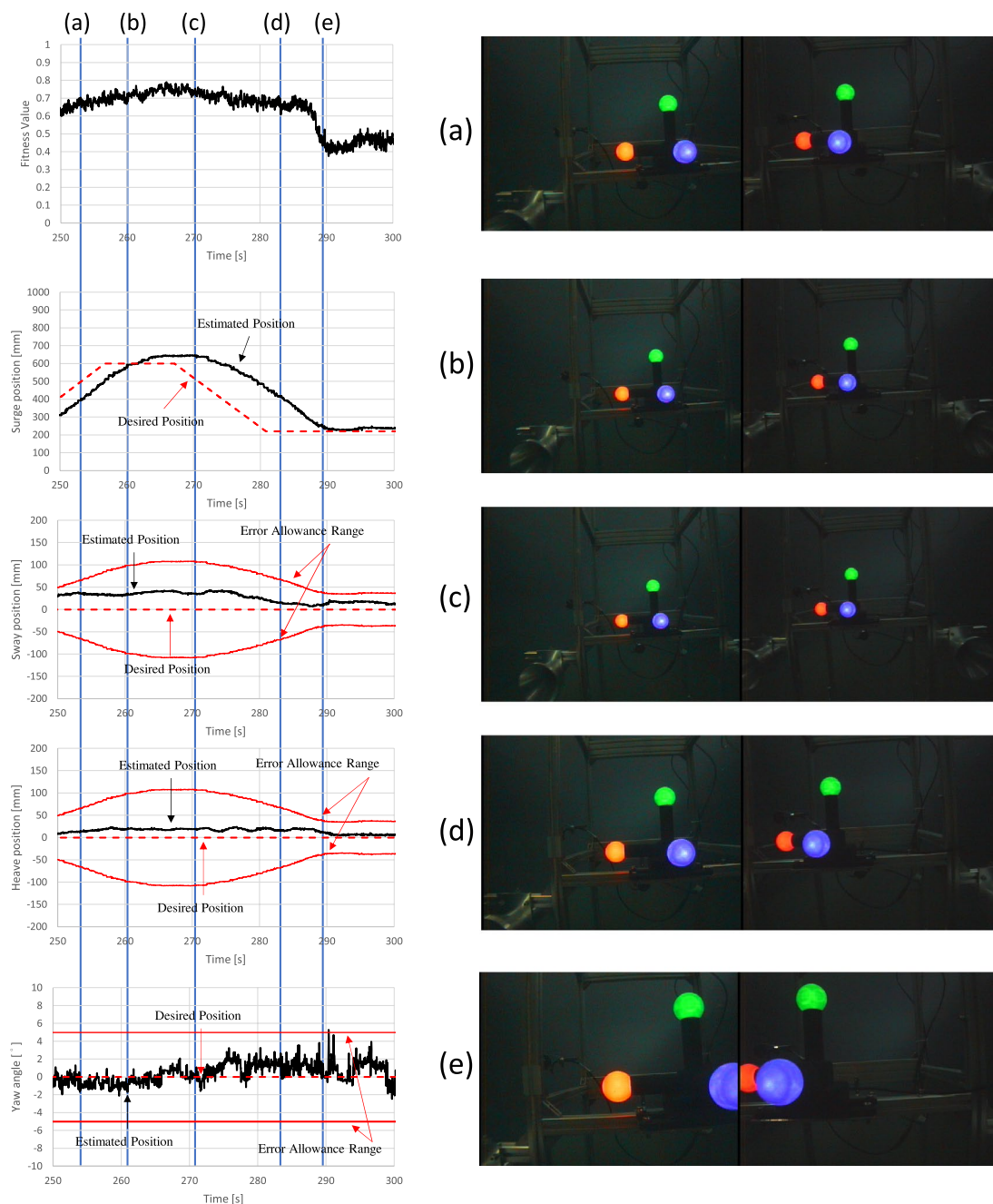


**Fig. 11** Images captured by the stereo-vision camera during the fourth iteration of docking

docking operation in this experiment are  $d_s = 800$  [mm] and  $d_f = 180$  [mm] respectively in the surge direction. The experimental result is also divided into five periods to be analyzed in detail, from Fig. 12a, e. Figure 12a shows the start of the docking operation. A few seconds later, a pole was inserted to impose an external force to the AUV, as shown in Fig. 13a. The direction of external force is shown by the red arrow. Figures 12b and 13(b) show

the moment AUV has been pushed. The external force causes displacement of the AUV, especially in the surge, sway and yaw direction. At this moment, the values of estimated positions in the surge, sway, and yaw direction are 863 [mm], 232 [mm], and  $16.3^\circ$  respectively. The values of estimated positions in the sway and yaw direction are out of the error allowance range. Thirty seconds later, the estimated positions in the surge and sway directions

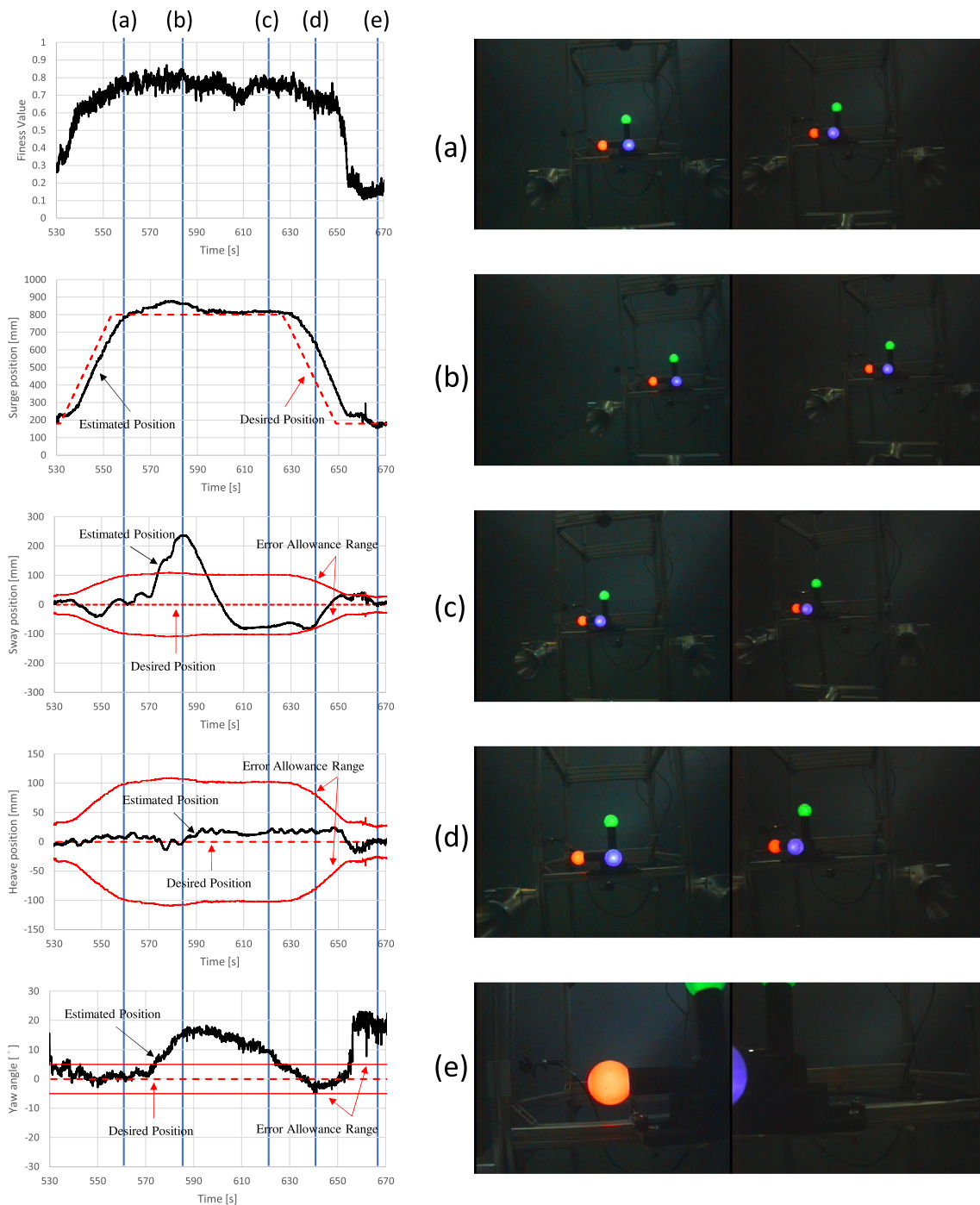


**Fig. 12** Experimental results of the second preliminary experiment

are recovered, and yaw is being recovered, as shown in Fig. 12c. Seeing that the thrusters on the AUV used to recover the estimated position in the sway and yaw affect one another, an error arises in the sway direction, in which the estimated position is -76.3 [mm]. A few seconds later, all the estimated positions are in the error allowance range; thus, the AUV starts to perform the docking operation, as

shown in Fig. 12d. In Fig. 12e, the docking operation is completed, but the fitness value is only 0.16, for the AUV is so close to the 3D marker that it cannot be completely photographed by the stereo-vision camera.

The results of the two preliminary experiments show that the proposed system applied to the AUV works properly.

**Table 3** Integrated INS error in the three docking operations

	Surge position	Sway position
First docking operation	867.6 [mm]	4.5 [mm]
Second docking operation	33.3 [mm]	- 33.5 [mm]
Third docking operation	33.3 [mm]	- 33.5 [mm]

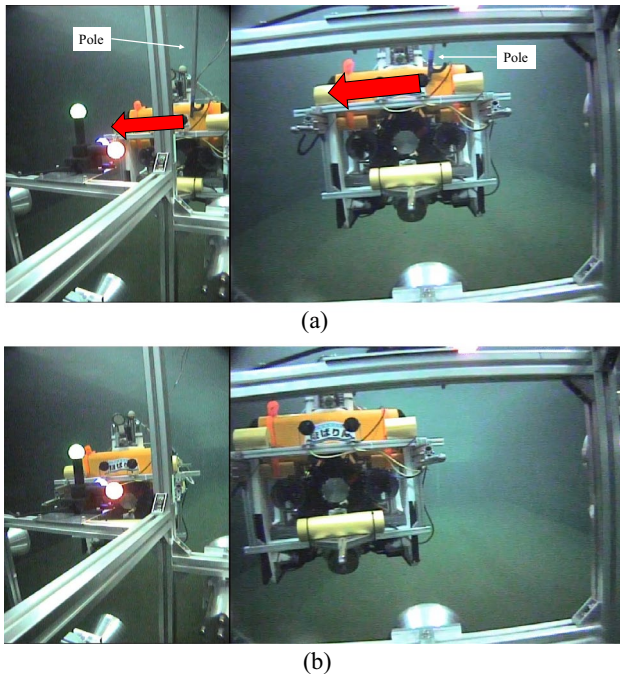


**Fig. 13** **a** A pole is used to make an external force applied to the AUV **b** The forces cause displacement of the AUV

### 4.3 Comprehensive experiment: recharging operation by means of AUV normal navigation system and the stereo-vision-based navigation system

The comprehensive experiments were conducted by the AUV returning to the docking station for recharging. In this experiment, the AUV normal navigation system is combined with the proposed system. Figure 14 shows the recharging operation from Phase 1 to Phase 6, which represents navigation-return-docking operations as shown in Fig. 14, and six phases have been repeated three times of navigation-return-docking operation. Regarding the mode of the control system, the AUV normal navigation system using the INS and DVL is set to Mode 30, and the proposed system is set to Mode 32. Figure 14 shows that, in Phase 1, the AUV uses the normal navigation system to approach the docking station and detect the presence of the 3D marker in the captured images. When the AUV detects the 3D marker (fitness value  $\geq 0.3$ ), the operating mode of the system changes from the normal navigation

system (Mode 30) to the proposed system (Mode 32). While using the proposed system, the position estimation of the normal navigation system is continuously working. In the docking mode, the AUV keeps an accurate pose that fulfills the docking conditions to perform the docking operation. After the docking operation is completed, the AUV moves away from the docking station and then prepares for the next docking operation. Figure 15 shows the flowchart of Phase 1 and Phase 2.

The experimental results of the position estimations of normal navigation system are shown in Fig. 16. Table 3 shows the integrated error of the position estimation by the normal navigation system in the three docking operations.

However, in the black circles shown in Fig. 16, the integrated error can be reset to 0 in the docking mode (Mode 32) because the position of the AUV is accurately known at the end of the successful docking operation. Figure 17 shows the experimental result of the first docking operation. The time to reset the integrated INS error ranges from 310 s, at which the docking phase is completed, to 350 seconds, at which the launching phase hasn't started yet.

In this experiment, the AUV with the proposed stereo-vision-based navigation system performs the docking operation in the battery recharging operation. In addition, the integrated INS error is reset after the docking operation is completed. Experimental results show that the proposed stereo-vision-based navigation system is capable of docking the AUV and resetting the integrated INS error.

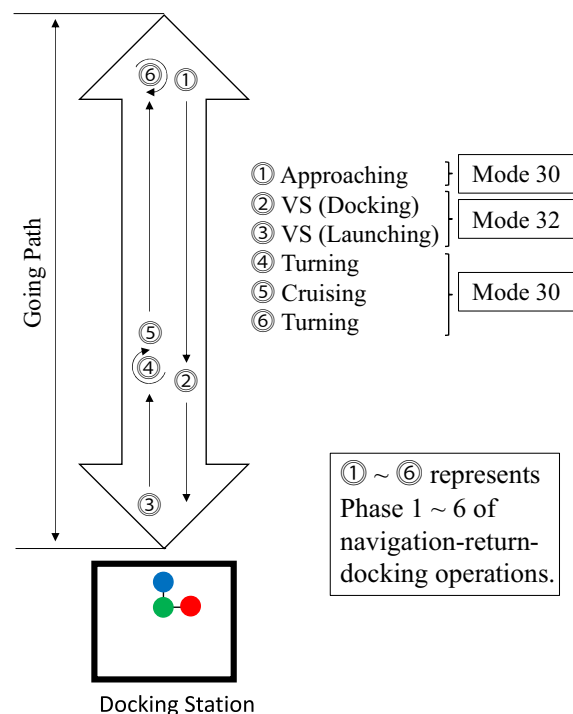


**Fig. 14** The operations for the comprehensive experiment

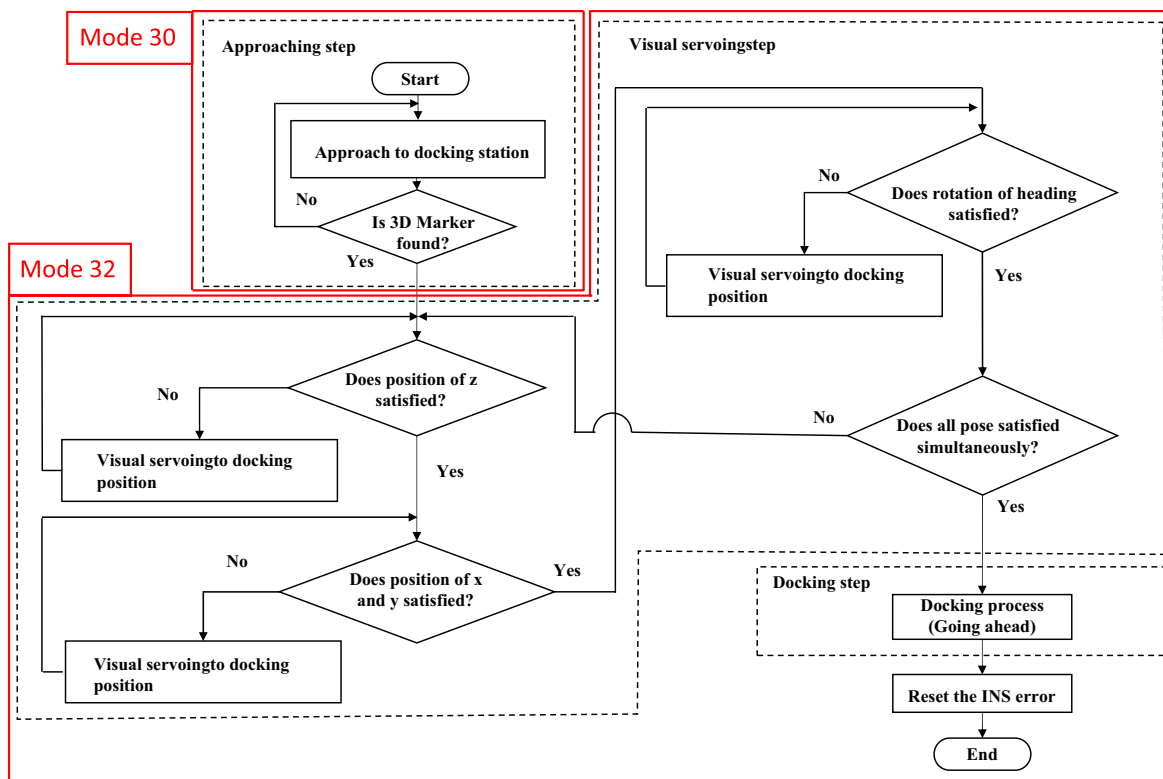


Fig. 15 The two types of mode switch when the AUV detects the 3D marker

### 5 Conclusion

In this study, we conducted the docking experiment of battery recharging in a test tank by means of the hovering-AUV. The AUV approached the docking station with the normal navigation system by INS and DVL, and automatically

performed the docking operation with only visual information from the stereo-vision camera. The experimental results show that the integrated INS error is reset after the AUV completes the docking operation. Further studies will be conducted to develop the proposed system in a real sea environment and then perform trials of docking an AUV and recharging the battery underwater.

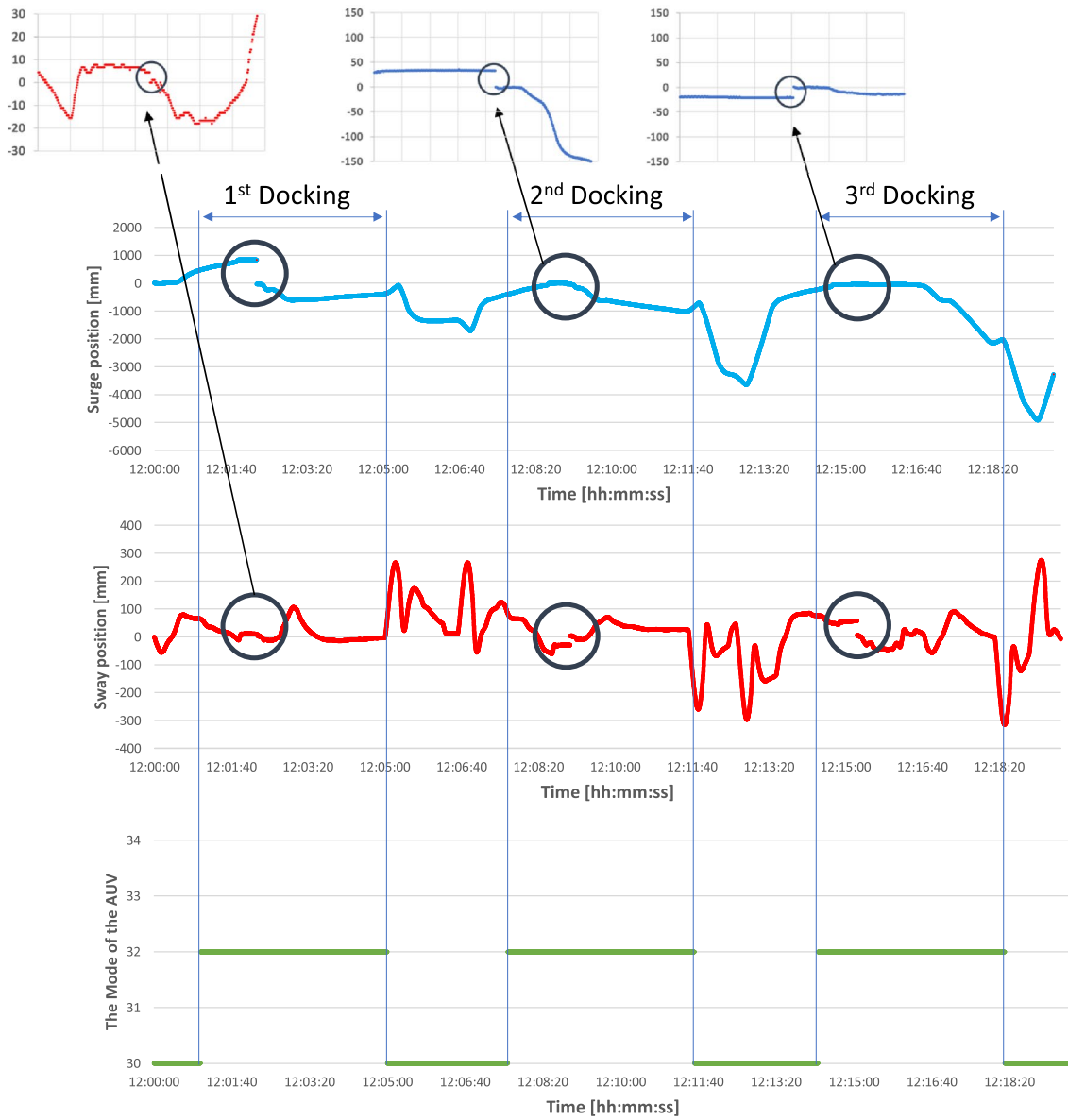
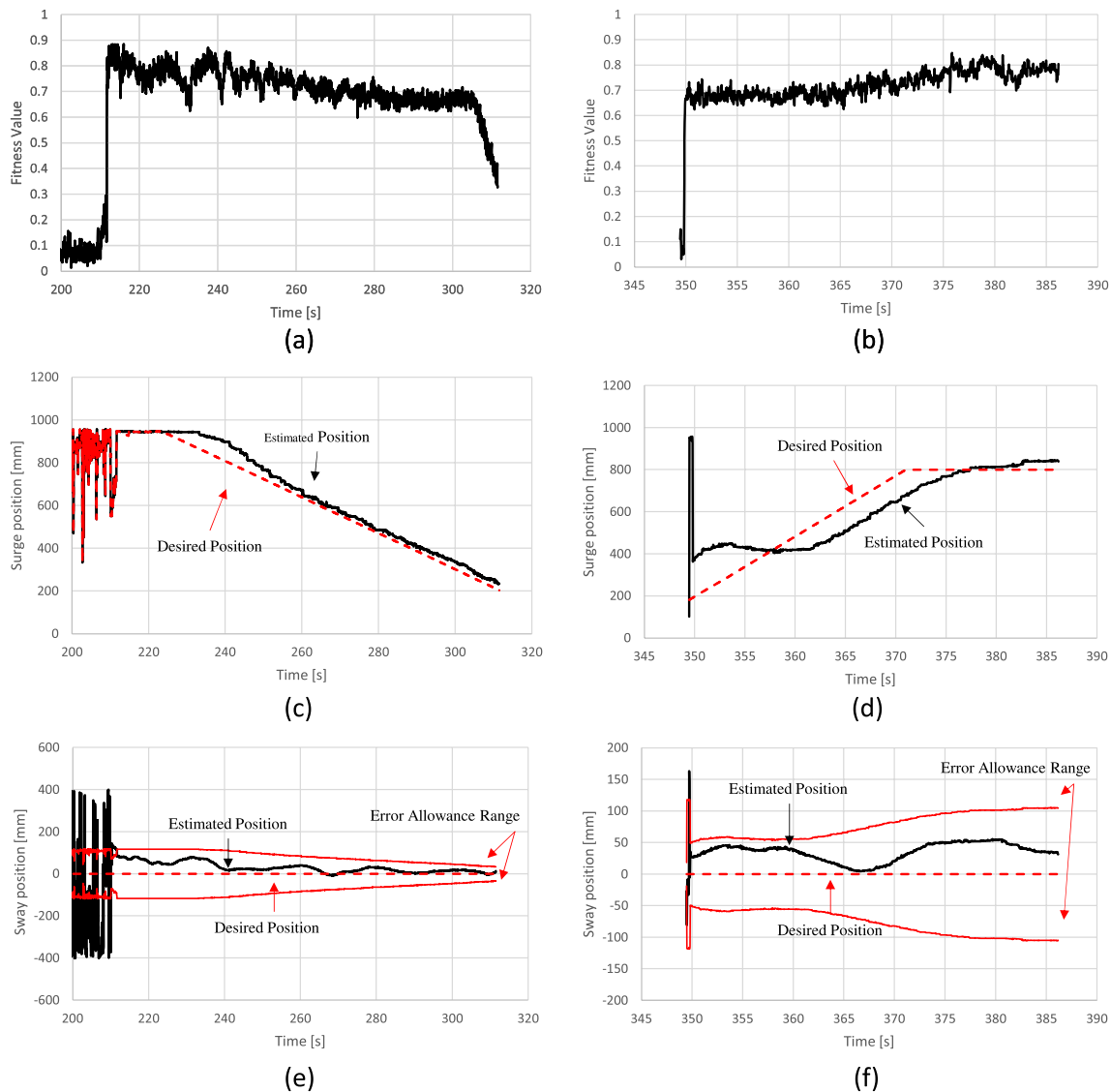


Fig. 16 Experimental result for the INS data



**Fig. 17** Experimental results for the first docking operation: (a) fitness value for docking, (b) fitness value for launching, (c) surge position for docking, (d) surge position for launching, (e) sway position for docking and (f) sway position for launching

**Acknowledgements** The AUV used in this work is supported by the Cross-ministerial Strategic Innovation Promotion Program (SIP), “Next-generation technology for ocean resources exploration” (Lead agency: Japan Agency for Marine-Earth Science and Technology, JAMSTEC).

## References

- Balasuriya BAAP, et al (1997) Vision based autonomous underwater vehicle navigation: underwater cable tracking. Oceans’ 97 MTS/IEEE Conference Proceedings: 1418-1424
- McEwen Robert S et al (2008) Docking control system for a 54-cm-diameter (21-in) AUV. IEEE J Oceanic Eng 33(4):550–562
- Narcis Palomeras et al (2014) I-AUV docking and intervention in a subsea panel. IEEE/RSJ Int Conf Intell Robots Syst 2014:2279–2285
- Morgado Marco, et al (2006) USBL/INS tightly-coupled integration technique for underwater vehicles. 2006 9th International Conference on Information Fusion: 1-8
- Hegrenæs *Øyvind*, and Oddvar Hallingstad, (2011) Model-aided INS with sea current estimation for robust underwater navigation. IEEE J Oceanic Eng 36(2):316–337
- Enric Galceran et al (2012) A real-time underwater object detection algorithm for multi-beam forward looking sonar. IFAC Proc Vol 45(5):306–311
- Cowen Steve, Susan Briest, James Dombrowski (1997) Underwater docking of autonomous undersea vehicles using optical terminal guidance. Oceans’ 97 MTS/IEEE Conference Proceedings: 1143-1147
- Ken Teo, Goh Benjamin, Chai Oh Kwee (2014) Fuzzy docking guidance using augmented navigation system on an AUV. IEEE J OceanicEng 40(2):349–361

9. Park Jin-Yeong, et al (2007) Experiment on underwater docking of an autonomous underwater vehicle 'ISiMI' using optical terminal guidance. OCEANS 2007-Europe: 1-6
10. Matthew Dunbabin, Lang Brenton, Wood Brett (2008) Vision-based docking using an autonomous surface vehicle. IEEE Int Conf Robotics Auto 2008:26–32
11. Myint Myo, et al (2015) Robustness of visual-servo against air bubble disturbance of underwater vehicle system using three-dimensional marker and dual-eye cameras. OCEANS 2015-MTS/IEEE Washington: 1-8
12. Nwe Lwin Khin et al (2019) Sea docking by dual-eye pose estimation with optimized genetic algorithm parameters. J Intell Robot Syst 96(2):245–266
13. Myint Myo, et al (2016) Visual-based deep sea docking simulation of underwater vehicle using dual-eyes cameras with lighting adaptation. OCEANS 2016-Shanghai: 1-8
14. Lwin Khin Nwe et al (2018) Visual docking against bubble noise with 3-D perception using dual-eye cameras. IEEE J Oceanic Eng 45(1):247–270
15. Horng-Yi Hsu et al (2019) Improving pose estimation accuracy and expanding of visible space of lighting 3D marker in turbid water. IEEE Underwater Technol 2019:1–8
16. Hsu Horng-Yi et al (2020) Visibility improvement in relation to turbidity and distance, and application to docking. Artif Life Robot 25(3):453–465
17. Myo Myint et al (2018) Dual-eyes vision-based docking system for autonomous underwater vehicle: an approach and experiments. J Intell Robot Syst 92(1):159–186
18. Okamoto Akihiro, et al (2016) Development of hovering-type AUV gHOBALIN h for exploring seafloor hydrothermal deposits. OCEANS 2016 MTS/IEEE Monterey: 1-4
19. Akihiro Okamoto et al (2019) Visual and Autonomous Survey of Hydrothermal Vents Using a Hovering Type AUV: Launching Hobalin Into the Western Offshore of Kumejima Island. Geochem Geophys Geosyst 20(12):6234–6243
20. Nwe Lwin Khin et al (2018) Docking at pool and sea by using active marker in turbid and day/night environment. Artificial Life Robot 23(3):409–419
21. Minami Mamoru, Julien Agbanhan, Toshiyuki Asakura (2003) Evolutionary scene recognition and simultaneous position/orientation detection. Soft computing in measurement and information acquisition: 178-207
22. Wei Song, Minami Mamoru, Aoyagi Seiji (2008) On-line stable evolutionary recognition based on unit quaternion representation by motion-feedforward compensation. Int J Intell Comput Med Scie Image Process 2(2):127–139
23. Nakamura Sho, et al (2018) Development of Dual-eyes Docking System for AUV with Lighting 3D Marker. OCEANS 2018 MTS/IEEE Charleston: 1-9

**Publisher's Note** Springer Nature remains neutral with regard to jurisdictional claims in published maps and institutional affiliations.